Numerical Investigation of Methods Used In Commercial Clinical Devices for Solving the ECGI Inverse Problem

Narimane Gassa, Vitaly Kalinin, Nejib Zemzemi

HAL Id: hal-04124322
https://hal.science/hal-04124322

Numerical Investigation of Methods Used In Commercial Clinical Devices for Solving the ECGI Inverse Problem

Narimane Gassa[1,3,4], Vitaly Kalinin[2], and Nejib Zemzemi[1,3,4][0000−0002−1212−8090]

[1] Institut de Mathématiques de Bordeaux UMR 5251 Talence France.
[2] EP Solutions SA. Yverdon-les-Bains, Switzerland.
[3] Centre INRIA de l'Université de Bordeaux, Talence, France.
[4] IHU-LIRYC, Pessac France.

Abstract. Electrocardiographic Imaging (ECGI) is a promising tool to non-invasively map the electrical activity of the heart using body surface potentials (BSPs) combined with the patient specific anatomical data. In this work, we assess two ECGI algorithms used in commercial ECGI systems to solve the inverse problem; the Method of Fundamental Solutions (MFS) and the Equivalent Single Layer (ESL). We quantify the performance of these two methods in conjunction with two different activation maps to estimate the activation times and earliest activation sites. ESL provided more accurate reconstruction of the cardiac electrical activity, especially on the endocardial part of the heart. Nevertheless, both methods provided comparable results in terms of the derived activation maps and the localization of the focal origin as a clinically relevant parameter.

Keywords: Inverse problem · Electrocardiography · Equivalent Single Layer · Method of Fundamental Solutions.

1 Introduction

The electrocardiographic imaging (ECGI) is a non-invasive technique that enables study of the body surface potentials for the treatment and diagnosis of cardiac arrhythmia. Heart activity is reconstructed from electrocardiograms measurements at the body surface and the patient specific heart-torso geometry. Mathematically, the problem is known as the inverse problem in electrocardiography. To date, several numerical methods have been used to solve the ECGI inverse problem. The most frequently used are the Finite Element Method (FEM; [3]), the Boundary Element Method (BEM; [2]), the Method of Fundamental Solution (MFS; [5]) and the equivalent single layer (ESL; [1]) source model. In a recent work of *Karoui et. al.* fifteen algorithms for the resolution of the ECGI inverse problem were evaluated; MFS and FEM were combined with different approaches to select the optimal regularization parameter in conjunction with zero order and L1-Norm Tikhonov regularization. The obtained results using experimental data indicate that MFS performs as well as FEM [6]. In contrast to FEM

that requires a full heart-torso discretized volume, MFS is a meshless method and does not require the torso geometry making a good compromise between accuracy and computational complexity. BEM is also a mesh-based method, where only a surface mesh is required, which reduces the computation time compared to FEM but may require more memory. On the other hand, a novel approach based on a representation of the electrical potential on the heart surface as ESL was proposed in [1] and showed promising results in the reconstruction of cardiac electrical activities.

A rigorous and theoretical justification of MFS and ESL can be found in [8]. For this study, we have implemented the MFS and ESL methods as described in the literature, and evaluated their numerical performance when used together with two different approaches for approximating activation times. Both simulated in silico data and clinical pacing data were included in our analysis.

2   Methods

2.1   Mathematical Modeling of the Inverse Problem

Let us suppose that Ω_{T} denotes the torso domain, Γ_{ext} is the external boundary, Γ is the heart-torso interface and u is the electrical potential in the torso governed by the diffusion equation. The inverse problem in electrocardiography for the geometry shown in Figure 1 is to find the electrical potential on the heart surface Σ satisfying both Dirichlet and Neumann boundary conditions such that:

$$\nabla \cdot (\sigma \nabla u) = 0, \quad \text{in } \Omega_T, \tag{1}$$

$$\sigma \nabla u \cdot n = 0 \text{ and } u = u_{\mathrm{T}}, \quad \text{on } \Gamma_{\mathrm{ext}}, \tag{2}$$

$$u = u_{\mathrm{H}}, \quad \text{on } \Sigma, \tag{3}$$

where u_{T} is the measured body surface potential and σ denotes the torso conductivity tensor. This is known as the forward problem in electrocardiography represented by a Cauchy problem for the Laplace equation to study the electrical activity of the heart through the body surface.

Given the heart and torso geometries combined with the measurements at the body surface, we express the Problem (1)-(3) in a matrix-vector system:

$$\mathbf{A}\mathbf{x} = \mathbf{b}, \tag{4}$$

where $\mathbf{A}$ is the transfer matrix, $\mathbf{b}$ is derived from u_{T} and $\mathbf{x}$ is the unknown variable from which it is possible to reconstruct u_{H}.

2.2   Method of Fundamental Solution (MFS)

In this method, we approach the solution of the Problem (1)-(3) with a linear combination of fundamental solutions of the differential operator which is, in our case, the *Laplacian*. These solutions are located on a set of virtual source points
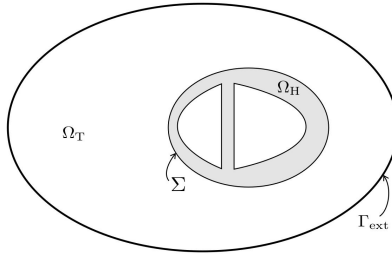
Fig. 1. The heart and torso domains: Ω_H and Ω_T.

$y_j, j = 1 \ldots M$ over an auxiliary surface as shown in [5]. The electrical potential is expressed as:

$$u(x) = a_0 + \sum_{i=1}^{M} f(x, y_j)\, a_j,$$

where $x \in \Omega_T$, y_j are the virtual source points and $a_j, j = 1 \ldots M$ are their corresponding coefficients. In this context, f represents the Laplace fundamental solution, which is explicitly defined as $f(r) = \frac{1}{4\pi r}$, with r being the Euclidean distance between two points x and y. When using Dirichlet and Neumann conditions we obtain the linear system $\mathbf{Ma} = \mathbf{d}$, with:

$$\mathbf{a} = (a_0, a_1, \cdots, a_M)^T,$$
$$\mathbf{d} = (u_{x_1}, \cdots, u_{x_N}, 0, \cdots, 0)^T,$$

and $\mathbf{M}$ is the transfer matrix.

2.3   Equivalent Single Layer (ESL)

Kalinin et. al. proposed a novel numerical approach to solve the inverse problem in electrocardiography. Furthermore, the paper [1] describes the following identity:

$$A = -H_{01} + G_{01}G_{11}^{-1}H_{11} \equiv 4\pi G_{01}G_{11}^{-1}, \tag{5}$$

where $q_0 = 0$, $q_1 = \frac{\partial u_1}{\partial n}$ and G_{ij}, H_{ij} are the matrices obtained from a discretization of the single- and double-layer integral operators in BEM, respectively. Given (5) we get

$$4\pi G_{01} \underbrace{G_{11}^{-1}u_1}_{w_1} = \underbrace{(H_{00} - G_{01}G_{11}^{-1}H_{10})}_{B} u_0. \tag{6}$$

Finally, the inverse problem of ECG can be formulated as follows:

$$4\pi G_{01}w_1 = Bu_0. \tag{7}$$

2.4   Activation Maps

Activation times are derived from the inverse computed electrograms.

Time of Inner Deflection (TID) The activation times are defined as the intrinsic deflection time at each point. Let $u_i(t)$ be the electrical potential at point x_i at time t, the activation time is:

$$\hat{T}_i = \operatorname*{argmin}_{t \in [0,T]} \frac{du_i(t)}{dt}. \tag{8}$$

Activation Direction Mapping (ADM) In this method, we first find the gradient field of the electrical potentials on the heart surface and then consider its projection on the tangential plane $g(x, t_k)$ for $x \in \Sigma$. On the heart surface, we calculate the vector function $\boldsymbol{A}(x)$ such that:

$$\boldsymbol{A}(x) = g(x, t_{k1}), \tag{9}$$

where

$$t_{k1} = \operatorname*{argmax}_{t_k} \left| g(x, t_k) \right|. \tag{10}$$

From the known function $\boldsymbol{A}$, we compute the scalar function $a(x)$ that minimizes the following functional:

$$I = \int_{\Sigma} |\nabla a - \boldsymbol{A}|. \tag{11}$$

Further details of this method can be found in [4].

3   Data

In order to assess the results obtained with the two proposed ECGI methods and quantify their performance, in-silico data were provided by EP-Solutions SA. The heart-torso geometry of three patients were derived from the Computer Tomography (CT) scans. Simulations were performed using the cardiac software CHASTE [7] and three focal type electrical activation patterns were simulated: in the lateral wall of the left ventricle (LV), in the right ventricular apex (RVA), and in the right ventricle outflow tract (RVOT). In addition, we used clinical data of three patients with two different and independent induced pacings in the right and left ventricular (RV and LV). The exact locations are known from the CT scans which will allow us to evaluate the excitation origin localization.

4   Evaluation

The comparison will mainly cover: i) The relative error (RE) between the true (simulated) and inverse computed (ic) electrogram. ii)The Pearson's correlation coefficient (CC) between the true and ic activation maps (both ADM and TID). iii)The localization error (LE) of the pacing site measured as the Euclidean distance between this latter and the ECGI based earliest activation site (EAS).

5 Results

5.1 Simulated Data

For the sake of example, we present in Figure 2 the inverse computed electrograms recorded at different locations in the heart during left ventricular pacing for geometry 1. The estimated accuracy metrics (re and cc) are indicated in Table 1.
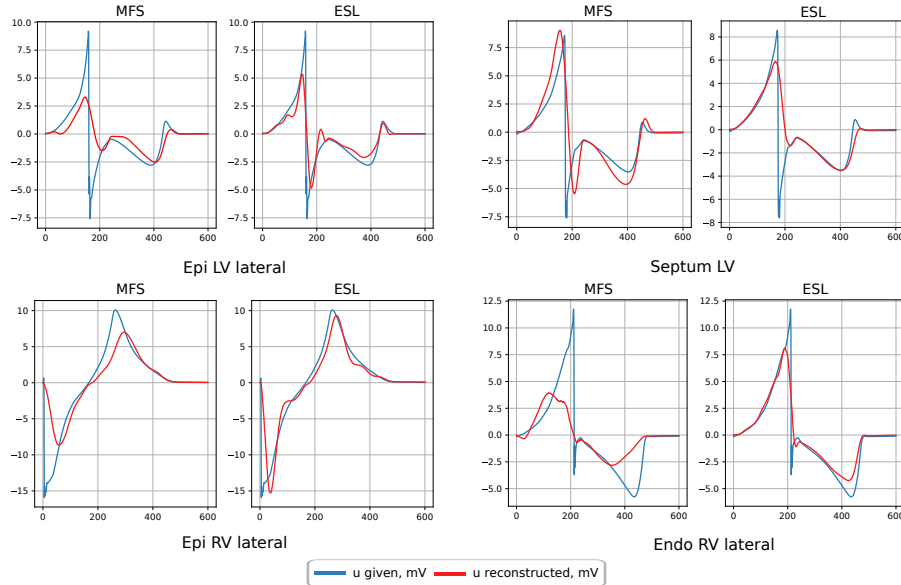

Fig. 2. Simulated (red line) and inverse reconstructed (blue line) electrograms at different sites of the endocardial and epicardial surfaces of the heart for a lateral LV pacing of geometry 1. The inverse solutions were obtained using MFS and ESL.

The results for the reconstructed signals in terms of relative errors are reported in Table 2 for the various test cases. In general, ESL results in a more accurate reconstruction of electrograms. The REs in average are equal to 0.58, 0.59, 0.53 for RVA, RVOT and LV cases, respectively. While MFS is less accurate for signal reconstruction with a relative error that varies between 0.70 and 0.81.

In Table 3, we report the values of the CC between the ground-truth (as derived from simulations) and *ic* activation maps for the four methods (MFS-TID, MFS-ADM, ESL-TID, ESL-ADM), the three stimulation protocols and the three geometries. Results show that all methods provide accurate reconstruction of the activation maps with a correlation coefficient ranging from 0.86 to 0.98, except when using TID for computing the left ventricular stimulation site in geometry 1.

Table 1. Estimated relative errors and correlation coefficients of the inverse reconstructed electrograms at different sites of the endocardial and epicardial surfaces of the heart for a lateral LV pacing of geometry 1. The inverse solutions were obtained using MFS and ESL.

	RE		CC	
Method	MFS	ESL	MFS	ESL
Epi LV lateral	0.49	0.46	0.86	0.89
Epi RV lateral	0.49	0.35	0.86	0.93
Septum LV	1.06	0.68	0.68	0.74
Endo RV lateral	0.67	0.30	0.90	0.96

Table 2. Spatial mean relative errors of the inverse reconstruted electrograms computed using MFS and ESL combined with TID and ADM for the different simulated pacing cases for the 3 geometries.

	RVA		RVOT		LV	
Method	MFS	ESL	MFS	ESL	MFS	ESL
Geometry 1	0.79	0.56	0.79	0.57	0.70	0.48
Geometry 2	0.81	0.62	0.85	0.62	0.75	0.54
Geometry 3	0.70	0.55	0.72	0.57	0.72	0.57

Table 3. Correlation coefficients between the exact and the inverse solution activation maps computed using MFS and ESL combined with TID and ADM for the different simulated pacing cases for the 3 geometries.

	RVA				RVOT				LV			
Method	MFS		ESL		MFS		ESL		MFS		ESL	
Act Map	ADM	TID	ADM	TID	ADM	TID	ADM	TID	ADM	TID	ADM	TID
Geometry 1	0.90	0.96	0.92	0.97	0.89	0.96	0.96	0.95	0.86	0.37*	0.97	0.33*
Geometry 2	0.91	0.94	0.91	0.96	0.92	0.94	0.95	0.95	0.93	0.96	0.95	0.98
Geometry 3	0.93	0.96	0.94	0.97	0.92	0.93	0.96	0.95	0.92	0.95	0.97	0.98

* This CC value is significantly lower than the average values.

In Table 4, we provide the localization errors of the pacing sites with respect to the inverse solution and the activation map reconstruction approach. The Mean±STD values of the localization errors using MFS-TID, MFS-ADM, ESL-TID and ESL-ADM methods, respectively, are 10.3 ± 4.5 mm, 10.2 ± 5.7 mm 6.8 ± 3.6 mm and 6.8 ± 3.1 mm.

Table 4. Localization errors in Millimeter between the exact and the inverse solution activation sites computed using MFS and ESL and combined with TID and ADM for the different simulated pacing cases for the 3 geometries.

Method	RVA				RVOT				LV			
	MFS		ESL		MFS		ESL		MFS		ESL	
Act Map	ADM	TID	ADM	TID	ADM	TID	ADM	TID	ADM	TID	ADM	TID
Geometry 1	6	2	8	6	9	14	11	13	13	15	3	4
Geometry 2	8	5	10	5	3	6	10	9	18	15	5	4
Geometry 3	11	5	4	5	10	18	10	10	15	12	1	6

5.2 Clinical Data

Due to the lack of electrical recordings that cover the surface of the heart in clinical cases, our only means of comparing our methods is by evaluating the localization error. In Table 5, we report the Euclidean LEs between the actual and earliest activation sites derived from the different activation maps. The Mean±STD values of the localization errors using MFS-TID, MFS-ADM, ESL-TID and ESL-ADM methods, respectively, are 42 ± 23 mm, 21 ± 7 mm 25 ± 25 mm and 16 ± 13 mm.

Table 5. Localization errors in Millimeter between the exact and the inverse solution activation sites computed using MFS and ESL and combined with TID and ADM for the LV and RV pacing cases for the 3 patients.

Method	Lateral RV				Lateral LV			
	MFS		ESL		MFS		ESL	
Act Map	ADM	TID	ADM	TID	ADM	TID	ADM	TID
Patient 1	10	72*	3	18	23	29	26	7
Patient 2	26	22	8	17	27	33	15	16
Patient 3	16	28	7	18	29	72*	37	76*

* This LE value is significantly lower than the average values.

In Figure 3, we show four examples of activation maps with respect to the inverse solution method and the activation map. Interestingly, ADM and TID yield visually very different maps. The use of TID based activation maps in clinical cases may induce more errors when we extract the earliest activation site, as shown in Table 5.
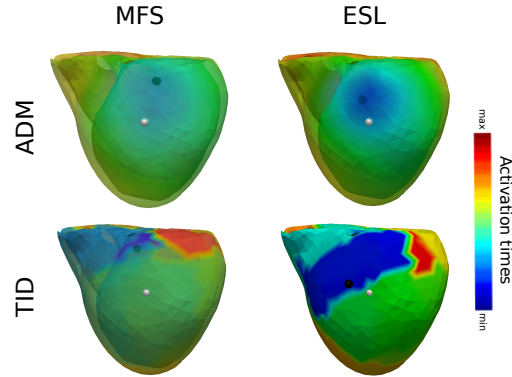
Fig. 3. Comparison of activation maps and pacing site localization with respect to the inverse solution method (MFS first column and ESL second column) and localization of early activation sites approach (ADM first row and TID second row). True activation sites are depicted in white and ECGI based activation sites are depicted in black.

6   Discussion and Conclusions

In this work, we evaluated the performance of two methods used in commercial medical devices for solving the electrocardiographic imaging inverse problem: the method of fundamental solutions and the equivalent single layer approach combined with two different approaches to compute activation times (TID and ADM). We tested the four possible combinations using simulated and clinical data. The evaluation of the different methods is based on the reconstruction of the heart surface potential and activation maps from simulated data and the localization of the pacing site from both simulated and clinical data.

For the in silico data-set, we used 3 different patient geometries and 3 cardiac paced rhythms: right-ventricular, left-ventricular and right-ventricular outflow tract pacing. In terms of signal reconstruction, ESL provided more accurate inverse solution in particular on the ventricular endocardial surface. Whereas, in terms of pacing site localization, both methods gave almost identical results with a slight difference for LV pacing.

The obtained LEs for clinical cases, indicate that ESL combined with ADM resulted in better localization accuracy and, in contrast to simulated data, TID and ADM based earliest activation sites can be very different. In fact, TID based activation maps is less robust to noisy and clinical data. This is mainly due to the fact that TID calculates activation times for each cardiac node separately (the point of maximum negative slope) without a spatial coherence. Consequently, in noisy data, it frequently provides patchy patterns in the obtained maps. However, activation direction mapping provides better results for clinical data despite the fact that it tends to over-smooth the spread of activation, which can be misleading in the excitation origin localization. The post-processing methods and in particular the activation times calculation have a significant impact on

ECGI and its usability in clinical applications. Thus, it would be interesting to work on cardiac activation maps that will better follow the temporal course of the inverse solution.

In this work, only single-paced rhythms were included. Therefore, further studies should include more complex activation patterns like ventricular tachycardia or atrial fibrillation.

Acknowledgments

References

1. Kalinin, A., Potyagaylo, D. and Kalinin, V., 2019. Solving the inverse problem of electrocardiography on the endocardium using a single layer source. Frontiers in physiology, p.58.
2. Barr, R.C., Ramsey, M. and Spach, M.S., 1977. Relating epicardial to body surface potential distributions by means of transfer coefficients based on geometry measurements. IEEE Transactions on biomedical engineering, (1), pp.1-11.
3. Wang, D., 2012. Finite element solutions to inverse electrocardiography. The University of Utah.
4. Denisov, A.M., Zakharov, E.V. and Kalinin, A.V., 2012. Method for determining the projection of an arrhythmogenic focus on the heart surface, based on solving the inverse electrocardiography problem. Mathematical Models and Computer Simulations, 4(6), pp.535-540.
5. Wang, Y. and Rudy, Y., 2006. Application of the method of fundamental solutions to potential-based inverse electrocardiography. Annals of biomedical engineering, 34(8), pp.1272-1288.
6. Karoui, A., Bear, L., Migerditichan, P. and Zemzemi, N., 2018. Evaluation of fifteen algorithms for the resolution of the electrocardiography imaging inverse problem using ex-vivo and in-silico data. Frontiers in physiology, 9, p.1708.
7. F.R. Cooper, R.E Baker, M.O. Bernabeu, R. Bordas, L. Bowler, A. Bueno-Orovio, H.M. Byrne, V. Carapella, L. Cardone-Noott, J. Cooper, S. Dutta, B.D. Evans, A.G. Fletcher, J.A. Grogan, W. Guo, D.G. Harvey, M. Hendrix, D. Kay, J. Kursawe, P.K. Maini, B. McMillan,G.R. Mirams, J.M. Osborne, P. Pathmanathan, J.M. Pitt-Francis, M. Robinson, B. Rodriguez, R.J. Spiteri, D.J. Gavaghan Chaste: Cancer, Heart and Soft Tissue Environment J. Open Source Softw. 5(47):1848, 2020. doi: 10.21105/joss.01848.
8. Kalinin, Vitaly, and Alexander Shlapunov. "Exterior extension problems for strongly elliptic operators: solvability and approximation using fundamental solutions." arXiv preprint arXiv:2209.11009 (2022).